Available online at www.sciencedirect.com
SCIENCE DIRECT®
Journal of Solid State Chemistry 178 (2005) 1683–1691
JOURNAL OF SOLID STATE CHEMISTRY
www.elsevier.com/locate/jssc

Hydrothermal synthesis of the perovskite manganites $Pr_{0.5}Sr_{0.5}MnO_3$ and $Nd_{0.5}Sr_{0.5}MnO_3$ and alkali-earth manganese oxides $CaMn_2O_4$, 4H-$SrMnO_3$, and 2H-$BaMnO_3$

Jeroen Spooren, Richard I. Walton*

Department of Chemistry, University of Exeter, Stocker Road, Exeter, EX4 4QD, UK

Received 11 February 2005; received in revised form 2 March 2005; accepted 6 March 2005

Abstract

We report the synthesis of the perovskite manganites $Pr_{0.5}Sr_{0.5}MnO_3$ and $Nd_{0.5}Sr_{0.5}MnO_3$ using mild hydrothermal conditions. Both are formed as polycrystalline powders from solutions of metal salts in aqueous potassium hydroxide at 240 °C, and crystallise as a tetragonal polymorph (space group $I4/mcm$). Scanning electron microscopy shows both materials to contain cuboid-shaped crystallites several microns in dimension, and the average particle size is verified by light scattering measurements. We also report the first hydrothermal synthesis of 2H-$BaMnO_3$ and 4H-$SrMnO_3$, and the first subcritical hydrothermal synthesis of $CaMn_2O_4$ (marokite). Despite the formation of these alkali-earth manganese oxides at 240 °C, we have been unable to isolate rare-earth manganese oxides $LnMnO_3$ using similar conditions. We discuss the formation of perovskite manganites in hydrothermal reactions by relating our new results to those manganites already reported to form under hydrothermal conditions, and rationalise the trends seen by considering tolerance factor of the perovskite and the variance of the *A*-site metal radius.

Keywords: Perovskites; Manganite

1. Introduction

For many years binary transition-metal oxides, such as Fe_3O_4 or TiO_2, have been prepared using solution methods, often via the hydrolysis of alkoxides or reactive chlorides under basic or acidic conditions close to room temperature [1]. The use of hydrothermal conditions, where an aqueous reaction mixture is heated above 100 °C in a sealed reaction container, permits a wider range of reaction conditions to be accessed for the synthesis of oxides. For example, under conditions of elevated temperature and autogenous pressure, the solubilities of starting materials and reagents can be very different than under ambient conditions, even before supercritical conditions are reached [2]. Furthermore, the mobilites of ions and other dissolved species are affected greatly by the changes in the dielectric constant and viscosity of water that occur with elevated pressure and temperature [2]. The hydrothermal method therefore has great potential for the preparation of materials that would usually be prepared using the traditional, high-temperature methods of solid-state chemistry: the use of a solvent would permit rapid mixing of several chemical elements, leading to homogeneous products, and also offers the potential for control of crystal growth leading to particles of desired morphologies, something rather difficult to achieve when using the high temperatures that must be employed in solid-state reactions. In particular, the hydrothermal method has great scope for the preparation of multinary oxide phases, i.e. containing two or more metals, where the rapid mixing of the constituent elements would provide a great synthetic advantage, as

*Corresponding author. Fax: +44 1392 263434.
E-mail address: r.i.walton@ex.ac.uk (R.I. Walton).

0022-4596/$ - see front matter © 2005 Elsevier Inc. All rights reserved.
doi:10.1016/j.jssc.2005.03.006

well as potentially leading to the discovery of new materials [3].

A number of ABO_3 perovskites have now been prepared using mild hydrothermal synthesis at remarkably low temperatures (less than 250 °C), compared to the usual high temperatures (greater than 1000 °C) used for the preparation of such materials. The titanates $BaTiO_3$ and $PbZr_xTi_{1-x}O_3$ (PZT) have been the most widely studied in this respect because of the considerable practical applications of the materials in electronic devices where their dielectric properties are exploited. Under hydrothermal conditions crystalline $BaTiO_3$ is formed at temperatures as low as 85 °C by reaction between basic solutions containing Ba^{2+} and either fine powders of the anatase polymorph of TiO_2 or amorphous hydrated TiO_2 [4–6]. For PZT, temperatures greater than 150 °C are generally employed in its hydrothermal synthesis, and a variety of metal sources have been employed, from amorphous mixed oxides of titanium and zirconium prepared by hydrolysis of the alkoxides [7] to distinct metal sources such as $ZrOCl_2$, $Pb(NO_3)_2$ and TiO_2 [8]. In the case of the hydrothermal synthesis of both $BaTiO_3$ and PZT, some control of particle size and particle morphology has been demonstrated: for example, Pinceloup et al. demonstrated that by addition of varying amounts of isopropanol to the hydrothermal synthesis of $BaTiO_3$, average crystallite size could be fine tuned between 30 and 100 nm [9], and in the case of PZT, Cho et al. have found that addition of tetramethylammonium hydroxide to the synthesis mixture allows crystal morphology to be adjusted from rod-like to cube-shaped [10]. Hydrothermal crystallisation mechanism has been investigated for $BaTiO_3$ and a number of distinct crystallisation pathways proposed [11] including dissolution-precipitation, where the starting materials dissolve completely and crystallisation takes place from solution [12], and the rearrangement of a mixed-metal gel phase formed early in the crystallisation [13].

Aside from $BaTiO_3$ and PZT, other perovskites that have been prepared using hydrothermal synthesis conditions include the titanates $SrTiO_3$ [14], $PbTiO_3$ [15] and $NaCe_{1-x}Nd_xTi_{2-y}V_yO_6$ [16], the zirconates $MZrO_3$ (M = Ca, Sr and Ba) [17,18], the niobate $NaNbO_3$ [19] and the tantalates $NaTaO_3$ [20] and $KTaO_3$ [21]. We [22,23] and others [24–29] have recently described the hydrothermal synthesis of the manganites $La_{0.5}M_{0.5}MnO_3$ (M = Ca, Sr, Ba). In this case, the synthesis is more challenging than the perovskites mentioned above, since control of manganese oxidation state is crucial in determining the materials' structures and properties. The hydrothermal synthesis of the lanthanum manganites takes place at temperatures between 240 and 275 °C in concentrated KOH solution and involves a comproportionation reaction between MnO_4^- and Mn^{2+} in the presence of lanthanum and alkali-earth metal salts to give the desired (average) manganese oxidation state of 3.5 at the beginning of the reaction [22,23]. The manganites are materials of great importance owing to their magnetic and electronic properties, particularly the phenomenon of colossal magnetoresistance [30,31]. We have therefore extended our hydrothermal synthetic method to investigate the preparation of manganites containing lanthanides other than lanthanum itself, and here report for the first time the successful hydrothermal synthesis of $Pr_{0.5}Sr_{0.5}MnO_3$ and $Nd_{0.5}Sr_{0.5}MnO_3$. We also describe hydrothermal synthesis of the chemically related manganese oxides $CaMn_2O_4$, $SrMnO_3$ and $BaMnO_3$ all of which have been prepared under mild hydrothermal conditions ($T < 240$ °C) for the first time.

2. Experimental section

Hydrothermal synthesis was undertaken using solutions of metal salts in aqueous potassium hydroxide. All chemicals were purchased from the Aldrich company and used as supplied: $KMnO_4$ (99%), $MnSO_4 \cdot H_2O$ (>98%), KOH pellets, $La(NO_3)_3 \cdot 6H_2O$ (99.99%), $BaCl_2 \cdot 2H_2O$ (>99%), $SrSO_4$ (anhydrous, >99%), $Ca(NO_3)_2 \cdot 4H_2O$ (99%), $Pr(NO_3)_3 \cdot 6H_2O$ (99.9%), $NdCl_3 \cdot 6H_2O$ (99.9%), Mn_2O_3 (300 mesh, 99%) and CaO (99.9%). The precise water content of each of the hydrated salts was checked by gravimetric analysis to allow accurate weighing of the materials, and the identity of the crystalline reagents was confirmed using powder X-ray diffraction. Since all reactions described in this work were successfully achieved at temperatures below 240 °C, all reactions were performed using 25 mL Teflon-lined, stainless-steel autoclaves. In order to ensure intimate mixing of reagents, solutions of the metal salts were prepared prior to mixing: 0.30 M $KMnO_4$, 0.35 M $MnSO_4$, 0.35 M $BaCl_2$, 0.35 M $Pr(NO_3)_3$ and 0.35 M $NdCl_3$. The solids $SrSO_4$, CaO, Mn_2O_3, and KOH were then weighed directly into the solution mixture as required and the mixture stirred for around 15 min. The typical percentage fill of the reaction vessel was 50%. After heating for the desired period of time and cooling to room temperature, solid products were recovered by suction filtration, washed with distilled water and dilute (1 M) nitric acid before being dried overnight at 50 °C in air. No post-synthesis annealing was undertaken.

Solids were analysed using powder X-ray diffraction, measured using a Bruker D8 diffractometer using Cu$K\alpha$ radiation (average $\lambda = 1.5418$ Å). Data were typically measured using a step-size of 0.02 °2θ, with a counting time of 10 s in Bragg-Bretano mode from powders pressed into aluminium plates. Data were analysed using the programs Celref [32] and Fullprof [33] which allowed refinement of cell parameters and calculation

of powder patterns from a structural model, respectively. Scanning electron microscopy was performed in order to evaluate crystallite size and morphology. This was undertaken using a Hitachi S-3200N instrument fitted with an Oxford Instruments INCA EDX analyser. Further and independent analysis of bulk average particle size and particle-size distribution was performed using light scattering with a Malvern Mastersizer S instrument from samples of solid suspended in ethylene glycol.

3. Results

3.1. The manganites $Pr_{0.5}Sr_{0.5}MnO_3$ and $Nd_{0.5}Sr_{0.5}MnO_3$

Table 1 shows some exploratory hydrothermal reactions aimed at synthesising praseodymium and neodymium manganites. The choice of KOH as mineraliser was based on prior work on the hydrothermal synthesis of the lanthanum manganites, where the use of other bases was unsuccessful [23]. For $Pr_{0.5}Sr_{0.5}MnO_3$ we found that if temperatures lower than 200 °C were used (e.g., Reaction 2 in Table 1), the desired product is always accompanied by large quantities of crystalline $Pr(OH)_3$ and $K_{0.5}Mn_2O_4 \cdot 1.5H_2O$. The same problem is encountered if reaction times of less than 24 h are employed (e.g., Reaction 3 in Table 1). Presumably in these situations the strontium not seen in crystalline products remains in solution. The pH of the solution is also crucial since at low KOH concentrations none of the desired product is observed and the impurities $Pr(OH)_3$ and $K_{0.5}Mn_2O_4 \cdot 1.5H_2O$ are accompanied by $PrMn_2O_5$ (e.g., Reaction 4 in Table 1). Identical behaviour was found for the synthesis of $Nd_{0.5}Sr_{0.5}MnO_3$ (entries 5–7, Table 1). Attempts to prepare $Ln_{1-x}Sr_xMnO_3$ with varying degrees of substitution level (i.e., the value of x) were always unsuccessful, and the recovered solid contained $Ln_{0.5}Sr_{0.5}MnO_3$ with $K_{0.5}Mn_2O_4 \cdot 1.5H_2O$ and $Ln(OH)_3$. In addition, reactions involving the lanthanides beyond neodymium (samarium, etc.) yielded no perovskite manganite phases.

Fig. 1 shows powder X-ray diffraction data for hydrothermal $Pr_{0.5}Sr_{0.5}MnO_3$ (produced in Reaction 1, Table 1) and hydrothermal $Nd_{0.5}Sr_{0.5}MnO_3$ (produced in Reaction 5, Table 1). In the latter case, a trace amount of $NdMn_2O_5$ is apparent (~1%), and it is probable that the 'missing' strontium has remained in solution, based on our observations above.

All of the Bragg peaks due to $Pr_{0.5}Sr_{0.5}MnO_3$ can be indexed using a tetragonal unit cell ($I4/mcm$) with refined cell parameters of $a = 5.3932(27)$ Å, $c = 7.7590(3)$ Å (see Supplementary Data for indexed data and figure of merit calculations for all powder diffraction data). This agrees well with the structural model proposed for a material of the same composition prepared by solid-state synthesis by Knížek et al. who found $a = 5.4038(3)$ Å, $c = 7.7872(5)$ Å [34] and by Damay et al. who found $a = 5.4031(1)$ Å, $c = 7.7879(2)$ Å [35]. Fig. 1(a) shows the calculated powder X-ray diffraction from this model (with our refined cell parameters) showing the excellent agreement with the experimental pattern. Woodward et al. used high-resolution synchrotron X-ray powder diffraction to study $Pr_{0.5}Sr_{0.5}MnO_3$ and were able to model their data as arising from a two-phase mixture of tetragonal $I4/mcm$ and orthorhombic $Imma$ phases, although the former was the major component (~85%) [36].

In the case of $Nd_{0.5}Sr_{0.5}MnO_3$, the powder X-ray diffraction data are also consistent with a tetragonal unit cell ($I4/mcm$) and our refined cell parameters are $a = 5.3785(27)$ Å, $c = 7.7696(1)$ Å. The agreement between the calculated and experimental data can be seen in Fig. 1(b). The volume of the unit cell of $Nd_{0.5}Sr_{0.5}MnO_3$ (224.8 Å^3) is slightly smaller than that of $Pr_{0.5}Sr_{0.5}MnO_3$ (225.7 Å^3) as expected with the slightly smaller radius of the Nd^{3+} cation. Interestingly,

Table 1
Reactions undertaken to investigate the hydrothermal synthesis of quaternary Pr- and Nd- containing manganites

Reaction	Reagent mixture	Temp./time	Crystalline products[a]
1	$0.3KMnO_4$:$0.7MnSO_4$:$0.5SrSO_4$:$0.5Pr(NO_3)_3$:107 KOH:$326H_2O$	240 °C/24 h	$Pr_{0.5}Sr_{0.5}MnO_3$
2	$0.3KMnO_4$:$0.7MnSO_4$:$0.5SrSO_4$:$0.5Pr(NO_3)_3$:$107KOH$:$326H_2O$	180 °C/24 h	$Pr_{0.5}Sr_{0.5}MnO_3$, $K_{0.5}Mn_2O_4 \cdot 1.5H_2O$[b], $Pr(OH)_3$[c]
3	$0.3KMnO_4$:$0.7MnSO_4$:$0.5SrSO_4$:$0.5Pr(NO_3)_3$:$107KOH$:$326H_2O$	240 °C/6 h	$Pr_{0.5}Sr_{0.5}MnO_3$, $K_{0.5}Mn_2O_4 \cdot 1.5H_2O$, $Pr(OH)_3$
4	$0.3KMnO_4$:$0.7MnSO_4$:$0.5SrSO_4$:$0.5Pr(NO_3)_3$:$9KOH$:$326H_2O$	240 °C/24 h	$PrMn_2O_5$[d], $K_{0.5}Mn_2O_4 \cdot 1.5H_2O$, $Pr(OH)_3$
5	$0.3KMnO_4$:$0.7MnSO_4$:$0.5SrSO_4$:$0.5NdCl_3$:$107KOH$:$326\ H_2O$	240 °C/24 h	$Nd_{0.5}Sr_{0.5}MnO_3$
6	$0.3KMnO_4$:$0.7MnSO_4$:$0.5SrSO_4$:$0.5NdCl_3$:$107KOH$:$326H_2O$	240 °C/6 h	$Nd_{0.5}Sr_{0.5}MnO_3$, $K_{0.5}Mn_2O_4 \cdot 1.5H_2O$, $Nd(OH)_3$[e]
7	$0.3KMnO_4$:$0.7MnSO_4$:$0.5SrSO_4$:$0.5NdCl_3$:$50KOH$:$326H_2O$	240 °C/24 h	$NdMn_2O_5$[f], $K_{0.5}Mn_2O_4 \cdot 1.5H_2O$, $Nd(OH)_3$, $Nd_{0.5}Sr_{0.5}MnO_3$

[a]On the basis of powder X-ray diffraction analysis.
[b]JCPDS card 87–1497.
[c]JCPDS card 75–1901.
[d]JCPDS card 88–0372.
[e]JCPDS card 70–0215.
[f]JCPDS card 88–0086.

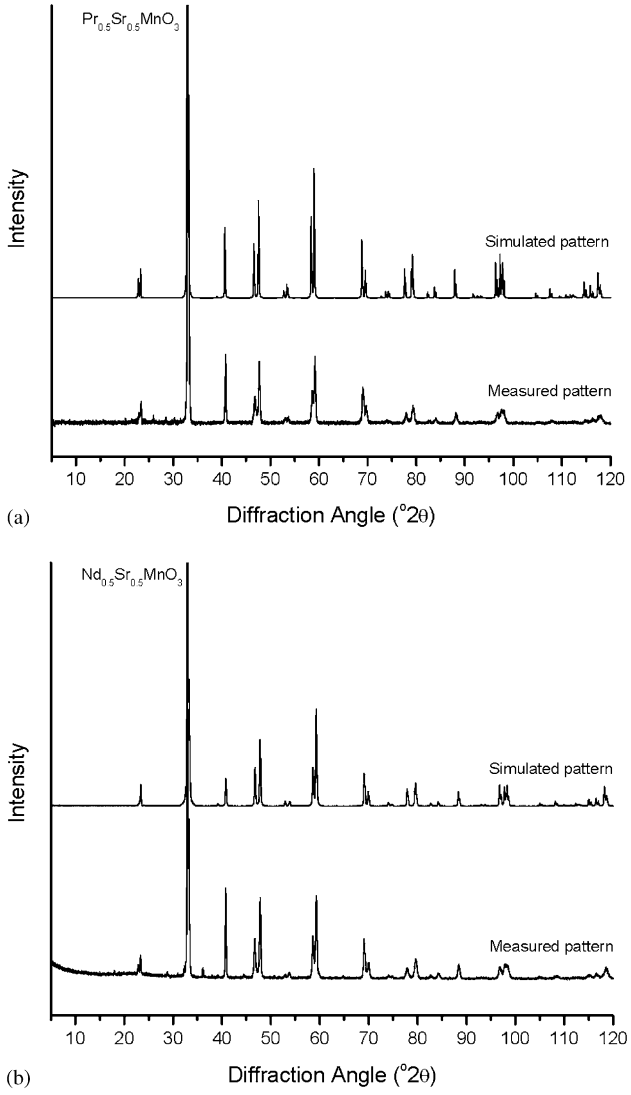

Fig. 1. Powder X-ray diffraction data from (a) $Pr_{0.5}Sr_{0.5}MnO_3$ and (b) $Nd_{0.5}Sr_{0.5}MnO_3$ prepared by hydrothermal synthesis.

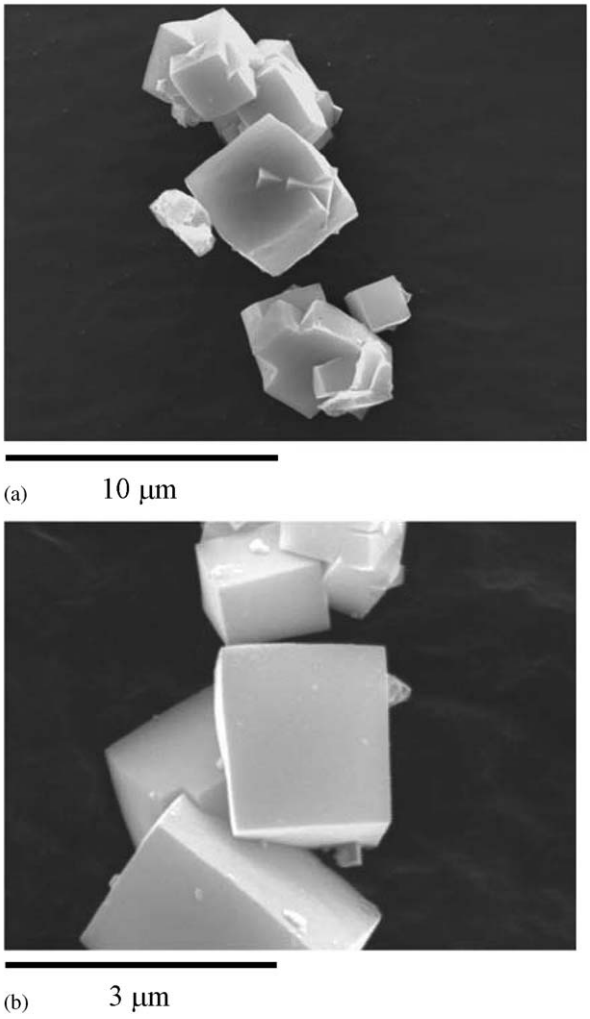

Fig. 2. Scanning electron micrographs of (a) $Pr_{0.5}Sr_{0.5}MnO_3$ and (b) $Nd_{0.5}Sr_{0.5}MnO_3$ prepared by hydrothermal synthesis.

others have previously reported an orthorhombic (*Imma*) unit cell for $Nd_{0.5}Sr_{0.5}MnO_3$ prepared by solid-state synthesis (>1400 °C) [36–38]. Given the rather similar radii of Nd^{3+} and Pr^{3+}, however, it is perhaps not surprising that the two manganites can adopt the same structure (note that Woodward et al. found $Pr_{0.5}Sr_{0.5}MnO_3$ to be a mixture of the tetragonal and orthorhombic polymorphs, showing the similar stability of the two forms [36]).

Scanning electron microscopy studies of hydrothermal $Pr_{0.5}Sr_{0.5}MnO_3$ and $Nd_{0.5}Sr_{0.5}MnO_3$ show the materials to be made up from small crystallites, around 5 μm in dimension, Fig. 2. Both materials consist of cuboid-shaped particles. Using the electron microscope EDXA of selected regions of the sample showed the presence of all three metals in every area analysed, in constant ratio. Light scattering measurements were performed to measure distributions of particle sizes in the bulk for both materials, Fig. 3. These show distributions of particle sizes in the range 1–10 μm, in both cases centred on around 5 μm, indicating the electron microscopy images to be representative of the bulk.

3.2. Alkali earth manganese oxides

Since we have successfully prepared a number of mixed-valent perovskite manganites of general formula $Ln_{0.5}A_{0.5}MnO_3$ (Ln = lanthanide ion and A = alkali earth ion) by hydrothermal synthesis in this and previous work [22,23], we were interested to determine whether it is possible to use similar methods to prepare the end members of the family, i.e. the materials of composition $LnMn^{III}O_3$ and $AMn^{IV}O_3$. This might allow us some understanding of the extent to which hydrothermal synthesis might be applied for the

preparation of complex manganese oxides with oxidation states +3, +4 or intermediate values. Table 2 shows the attempted synthesis undertaken, along with the products identified by powder X-ray diffraction.

The successful hydrothermal synthesis of $SrMnO_3$ and $BaMnO_3$ was achieved at 240 °C (Reactions A and B in Table 2). Fig. 4a shows powder X-ray diffraction data of $BaMnO_3$ and all Bragg peaks can be indexed using the structural model of Cussen and Battle ($P6_3/mmc$) [39]. Our refined unit cell parameters of $a = 5.7000(12)$ Å, $c = 4.8169(1)$ Å are consistent with the prior structure determination ($a = 5.7045(11)$ Å and $c = 4.8200(1)$ Å) for 2H-$BaMnO_3$. This material contains chains of face-sharing $\{MnO_6\}$ units, rather than the familiar perovskite structure where the $\{MnO_6\}$ units are corner-shared. $SrMnO_3$ also has hexagonal symmetry ($P6_3/mmc$, $a = 5.4565(24)$ Å, $c = 9.1017(1)$ Å), Fig. 4b, but its structure is made up of dimers of face-shared $\{MnO_6\}$ units, linked by corners [40]. Fig. 5a shows a scanning electron microscope image of our 2H–$BaMnO_3$ sample, showing the presence of tablet shaped crystallite with length ranging from ~0.5 to 2 μm. EDXA showed the particles to all contain Ba and Mn in the expected ratio. $SrMnO_3$ contains blade-shaped crystallite of a variety of sizes, as shown in Fig. 5b (EDXA showed that the smaller, less well-formed particles contained Sr and Mn in the correct ratio, the same as observed in the larger particles). We were not able to prepare $CaMnO_3$ using analogous hydrothermal reactions (see Reaction C, Table 2), but in the course of our attempts, we discovered that it is possible to prepare the manganese (III) oxide $CaMn_2O_4$ as a phase-pure sample by direct reaction between CaO and Mn_2O_3 in aqueous KOH at 240 °C (Reaction D, Table 2). Fig. 4c shows the powder X-ray diffraction data along with those calculated from the structural model of Zouari et al. [41] Our refined unit cell parameters ($a = 3.1569(32)$ Å, $b = 9.9991(58)$ Å, $c = 9.6670(63)$ Å) agree very well with those previously recently reported ($a = 3.1492(6)$ Å, $b = 9.98(2)$ Å, $c = 9.66(2)$ Å) for a sample prepared by solid-state synthesis [41]. The peak intensities of the powder diffraction data of $CaMn_2O_4$ are affected somewhat by preferred orientation, and this is consistent with the anisotropic shape of the crystallites. Scanning electron microscopy, Fig. 5c, of the hydrothermal $CaMn_2O_4$ sample shows the material to be made up of agglomerates of needle-shaped particles around 10 μm in length.

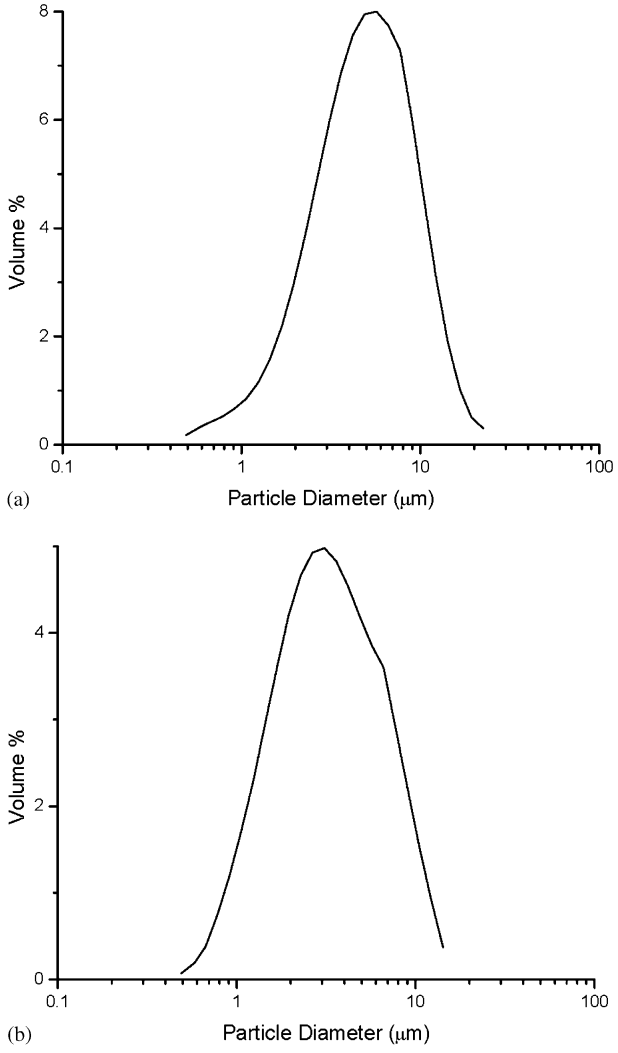

Fig. 3. Particle size distributions as obtained by light scattering for (a) $Pr_{0.5}Sr_{0.5}MnO_3$ and (b) $Nd_{0.5}Sr_{0.5}MnO_3$.

Using mild hydrothermal conditions at high pH we have not been able to synthesise any of the lanthanide

Table 2
Hydrothermal reactions undertaken to investigate the preparation of ternary alkali-earth manganese oxides and lanthanide manganese oxides

Reaction	Reagent mixture	Temp./time	Crystalline products[a]
A	$1BaCl_2$:0.4$KMnO_4$:0.6$MnSO_4$:180KOH:250H_2O	240 °C/24 h	$BaMnO_3$
B	$1SrSO_4$:0.4$KMnO_4$:0.6$MnSO_4$:125KOH:250H_2O	240 °C/24 h	$SrMnO_3$
C	$1Ca(NO_3)_2$:0.4$KMnO_4$:0.6$MnSO_4$:180KOH:250H_2O	240 °C/24 h	$Ca(OH)_2$, $K_{0.5}Mn_2O_4 \cdot 1.5H_2O$
D	CaO: Mn_2O_3:50KOH:200H_2O	240 °C/6 h	$CaMn_2O_4$
E	$1La(NO_3)_3$:0.2$KMnO_4$:0.8$MnSO_4$:180KOH:250H_2O	240 °C/24 h	$La(OH)_3$, $K_{0.5}Mn_2O_4 \cdot 1.5H_2O$
F	$1Pr(NO_3)_3$:0.2$KMnO_4$:0.8$MnSO_4$:180KOH:250H_2O	240 °C/24 h	$Pr(OH)_3$, $K_{0.5}Mn_2O_4 \cdot 1.5H_2O$
G	$1Nd(NO_3)_3$:0.2$KMnO_4$:0.8$MnSO_4$:180KOH:250H_2O	240 °C/24 h	$Nd(OH)_3$, $K_{0.5}Mn_2O_4 \cdot 1.5H_2O$

[a]On the basis of powder X-ray diffraction analysis.

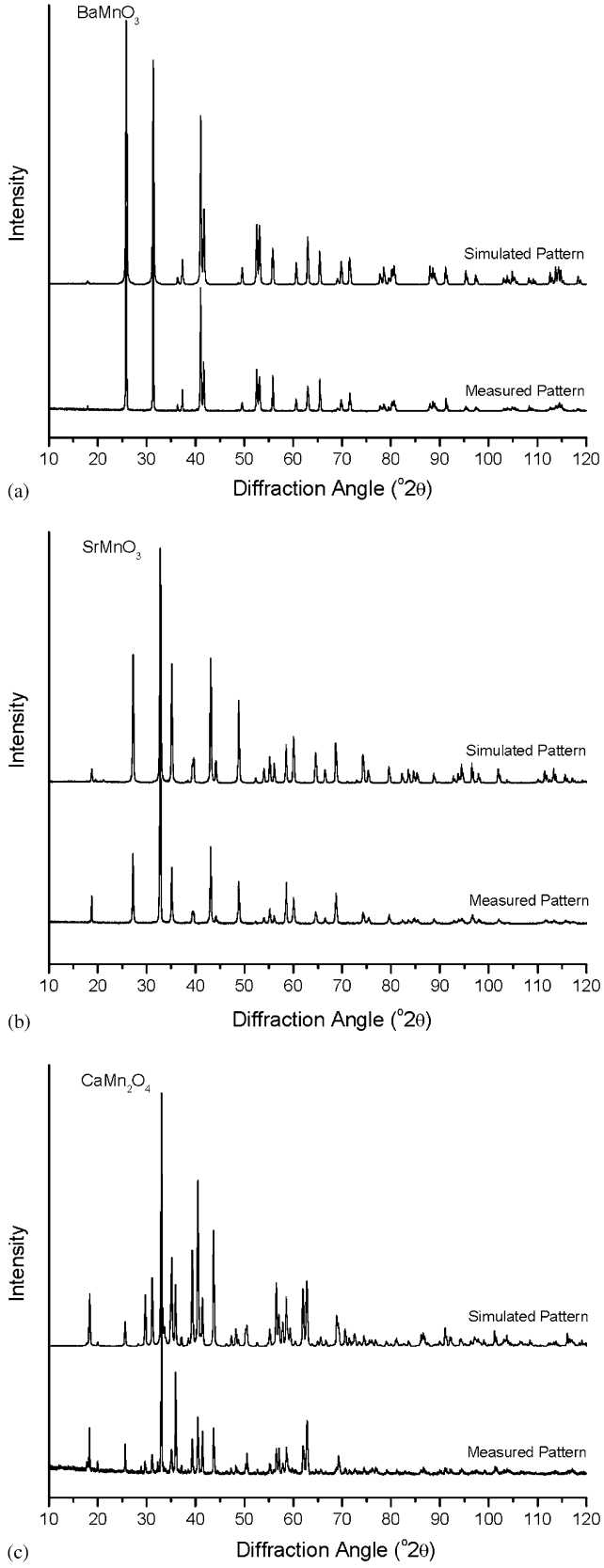

Fig. 4. Powder X-ray diffraction data from samples of (a) $BaMnO_3$ (b) $SrMnO_3$ and (c) $CaMn_2O_4$ prepared by hydrothermal synthesis.

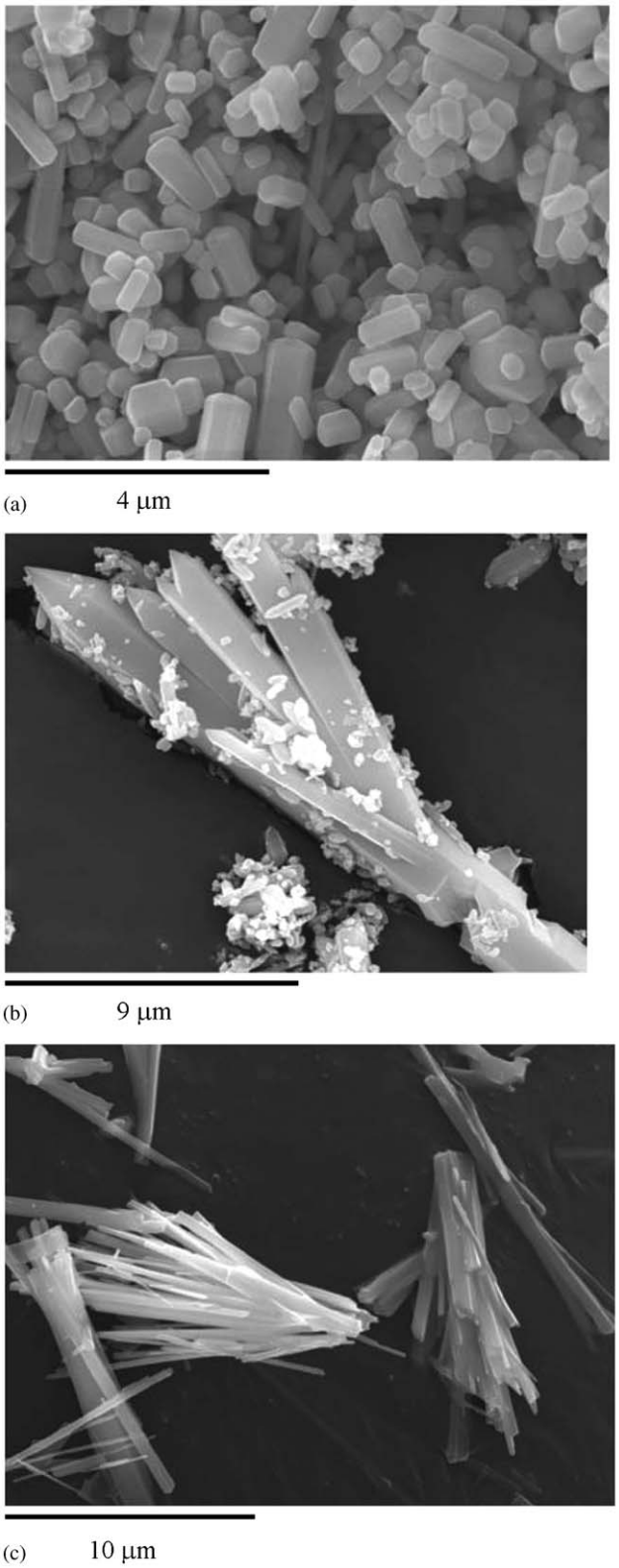

Fig. 5. Scanning electron micrographs of (a) $BaMnO_3$ and (b) $SrMnO_3$ and (c) $CaMn_2O_4$ prepared by hydrothermal synthesis.

manganese oxides $LnMn^{III}O_3$. Reactions conditions (temperature, time, pH, and choice of reagents) were varied over a large range and entries E to G in Table 2 are examples typical reactions investigated. Note in these cases we have used our protocol of mixing MnO_4^- and Mn^{2+} in the ratio 0.2:0.8 so to give the desired oxidation state of +3 in the reaction mixture. In all cases the solid product contained crystalline lanthanide hydroxide and $K_{0.5}Mn_2O_4 \cdot 1.5H_2O$.

4. Discussion and conclusions

We have successfully used hydrothermal synthesis to produce the manganites $Ln_{0.5}Sr_{0.5}MnO_3$ ($Ln = Pr$, Nd). The method allows these complex oxides to be formed in one step at considerably lower temperatures than typically employed in their synthesis. As previously found for the materials with $Ln = La$, we have been unable to prepare $Ln_{1-x}Sr_xMnO_3$ (Ln = Nd, Pr) phases with $x > 0.5$ and $x < 0.5$. As we have previously discussed for the case where $Ln = La$, this is most likely due to the formation of a poorly crystalline precursor phase, $K_{0.5}MnO_2 \cdot nH_2O$ prior to the crystallisation of the manganite, even when varying amounts of MnO_4^- and Mn^{2+} are used in the synthesis. The presence of the precursor phase forces the formation of the manganite with the same average oxidation state (+3.5), along with impurities such as $BaMnO_3$, $Ln(OH)_3$ and $LnMn_2O_5$ [23].

Table 3 shows the manganites now prepared by hydrothermal synthesis, along with some pertinent structural data. One widely used method of classifying perovskite structures is to use the tolerance factor first introduced by Goldschmidt [42]: this is listed in Table 3 for each material. We have also listed in Table 3 the variance in radius of the A-site metals for each material; this parameter has also found to be an important parameter in rationalising structure-property relationships in perovskites [43], and can provide complementary information to that described by the tolerance factor (which quantifies the mismatch between the mean radii of the A- and B-site metals). We have plotted the data from Table 3 on Fig. 6, along with the parameters for materials that we have been *unable* to synthesise using mild hydrothermal conditions ($T < 270\,^\circ C$); this includes the materials $Ln_{0.5}Ba_{0.5}MnO_3$ for $Ln = Pr$, Nd, the phases $Ln_{0.5}Ca_{0.5}MnO_3$ for $Ln = Pr$, Nd, and the end members $LnMnO_3$ (for all lanthanides). (In exploratory hydrothermal synthesis we varied pH and reagent concentration over a wide range in attempts to prepare these other manganite families.) It may be observed that the materials successfully prepared using low temperature hydrothermal conditions are those with tolerance factor close to 1 ($t > 0.9$) and with the smallest A-site radius variance ($\sigma^2(r_A) < 0.02\,\text{Å}^2$). Fig. 6 thus shows a region of tolerance/average A-site radius variance where the manganite perovskites can be prepared at low temperatures offered by hydrothermal synthesis. This connection between structural chemistry of perovskites and their synthesis has been made previously by others. For example, in the case of the rare-earth, alkali-earth manganites, Laberty et al. measured the enthalpies of formation of a series of perovskite manganites and determined a strong correlation between the enthalpy of formation and the tolerance factor: in particular those manganites with tolerance factor closest to unity had the most exothermic ΔH_f [44]. This relationship was also previously shown for $A^{2+}B^{4+}O_3$ perovskites in general [45].

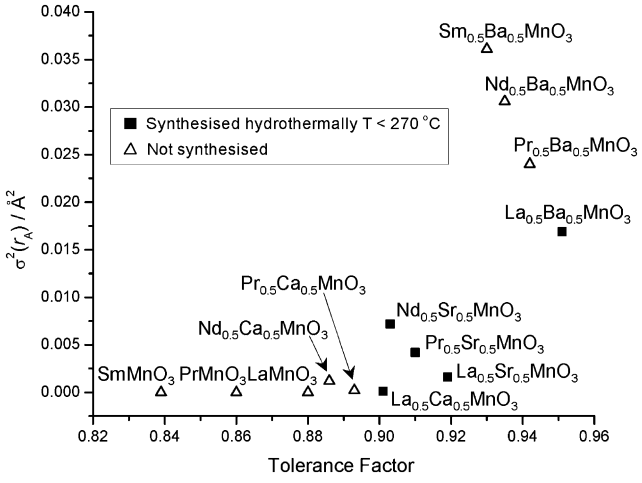

Fig. 6. Tolerance factor against A-site radius variance for manganites whose hydrothermal synthesis has been investigated.

Table 3
$Ln_{0.5}A_{0.5}MnO_3$ manganites prepared by hydrothermal synthesis

Material	Synthesis temperature (°C)	Reference	Tolerance factor[a]	A-site radius variance[a]
$La_{0.5}Ba_{0.5}MnO_3$	240	[22–25,27,29]	0.951	0.0169
$La_{0.5}Sr_{0.5}MnO_3$	240	[22,23,25,27]	0.919	0.0016
$La_{0.5}Ca_{0.5}MnO_3$	265–275	[23,28]	0.901	0.0001
$Pr_{0.5}Sr_{0.5}MnO_3$	240	This work	0.910	0.0042
$Nd_{0.5}Sr_{0.5}MnO_3$	240	This work	0.903	0.0072

[a]Calculated using the ionic radii of Shannon [50].

Rørmark et al. have subsequently found similar results from calorimetry for both $A^{3+}Mn^{3+}O_3$ and $A^{2+}Mn^{4+}O_3$ perovskites [46], and showed the same correlation between tolerance factor and enthalpy of formation for both series of materials. It is clear from these results that the energetics of formation of a manganite perovskite can depend on subtle details of its structure and composition, and this might go towards explaining why the use of mild hydrothermal conditions does not allow access to all possible manganite compositions.

Aside from considerations of the energetics of formation of the phases studied, our inability to prepare manganites of lanthanides beyond neodymium could also be explained by the decreasing solubility of the lanthanide hydroxide as the ionic radius of the Ln^{3+} ion decreases [47]. Since we must use a high concentration of KOH to achieve crystallisation of the manganites (possibly due to the formation of a potassium manganese oxide precursor, as discussed above), then crystallisation of the insoluble $Ln(OH)_3$ material would represent a 'dead-end' in the reaction, explaining why we cannot isolate the manganite for lanthanides beyond neodymium.

Finally we note that our successful synthesis of 2H-$BaMnO_3$ and 4H-$SrMnO_3$ represent the first reported hydrothermal synthesis of hexagonal ABO_3 materials. These materials, which have structures rather different than the perovskite structure, have previously been prepared exclusively by high-temperature, solid-state synthesis. Interestingly, $CaMnO_3$, which we cannot prepare using hydrothermal conditions (despite varying pH and starting materials over a wide range), is expected to adopt an orthorhombic distorted perovskite structure [48]. In the case of $CaMn_2O_4$, a synthetic example of the mineral marokite, a previous hydrothermal synthesis has been reported, but this used rather more severe conditions than we have found necessary: 600 °C for 3 days in a sealed silver tube [49].

Acknowledgments

We thank the EPSRC for funding, and access to the particle size instrument through their equipment pool. We are grateful to Mr. Christopher Wright for his assistance in obtaining one of the SEM images.

Appendix A. Supplementary Data

The online version of this article contains additional supplementary data. Please visit doi:10.1016/j.jssc.2005.03.006.

References

[1] J.-P. Jolivet, Metal Oxide Chemistry and Synthesis, Wiley, New York, 2003.
[2] A. Rabenau, Angew. Chem. Int. Ed. Engl. 24 (1985) 1026.
[3] R.I. Walton, Chem. Soc. Rev. 31 (2002) 230.
[4] W. Hertl, J. Am. Ceram. Soc. 71 (1988) 879.
[5] P.K. Dutta, J.R. Gregg, Chem. Mater. 4 (1992) 843.
[6] I.J. Clark, T. Takeuchi, N. Ohtori, D.C. Sinclair, J. Mater. Chem. 9 (1999) 83.
[7] M. Traianidis, C. Courtois, A. Leriche, B. Thierry, J. Eur. Ceram. Soc. 19 (1999) 1023.
[8] Y. Deng, L. Liu, Y. Cheng, C.-W. Nan, S.-J. Zhao, Mater. Lett. 57 (2003) 1675.
[9] P. Pinceloup, C. Courtois, J. Vicens, A. Leriche, B. Thierry, J. Eur. Ceram. Soc. 19 (1999) 973.
[10] S.-B. Cho, M. Oledzka, R.E. Riman, J. Cryst. Growth 226 (2001) 313.
[11] J.O. Eckert, C.C. Hung-Houston, B.L. Gersten, M.M. Lencka, R.E. Riman, J. Am. Ceram. Soc. 79 (1996) 2929.
[12] R.I. Walton, F. Millange, R.I. Smith, T. Hansen, D. O'Hare, J. Am. Chem. Soc. 123 (2001) 12547.
[13] A. Testino, M.T. Buscaglia, V. Buscaglia, M. Viviani, C. Bottino, P. Nanni, Chem. Mater. 16 (2004) 1536.
[14] C. Chen, X. Jiao, D. Chen, Y. Zhao, Mater. Res. Bull. 36 (2001) 2119.
[15] D. Chen, R. Xu, J. Mater. Chem. 8 (1998) 965.
[16] C.S. Wright, R.I. Walton, D. Thompsett, J. Fisher, Inorg. Chem. 43 (2004) 2189.
[17] W. Zheng, W. Pang, G. Meng, Solid State Ionics 108 (1998) 37.
[18] T.R.N. Kutty, R. Vivekanandan, S. Philip, J. Mater. Sci. 25 (1990) 3649.
[19] G.K.L. Goh, F.F. Lange, S.M. Haile, C.G. Levi, J. Mater. Res. 18 (2003) 338.
[20] Y. He, Y. Zhu, N. Wu, J. Solid State Chem. 177 (2004) 3868.
[21] Y. He, Y.F. Zhu, N.Z. Wu, J. Solid State Chem. 177 (2004) 2985.
[22] J. Spooren, A. Rumplecker, F. Millange, R.I. Walton, Chem. Mater. 15 (2003) 1401.
[23] J. Spooren, R.I. Walton, F. Millange, J. Mater. Chem. 2005, in press, doi:10.1039/b417003b.
[24] D. Wang, R. Yu, S. Feng, W. Zheng, G. Pang, H. Zhao, Chem. J. Chin. Univ. 19 (1998) 165.
[25] D. Zhu, H. Zhu, Y. Zhang, Appl. Phys. Lett. 80 (2002) 1634.
[26] D.L. Zhu, H. Zhu, Y.H. Zhang, J. Cryst. Growth 249 (2003) 172.
[27] J. Liu, H. Wang, M. Zhu, B. Wang, H. Yan, Mater. Res. Bull. 38 (2003) 817.
[28] T. Zhang, C.G. Jin, T. Qian, X.L. Lu, J.M. Bai, X.G. Li, J. Mater. Chem. 14 (2004) 2787.
[29] J.J. Urban, L. Ouyang, M.-H. Jo, D.S. Wang, H. Park, Nano Letters 4 (2004) 1547.
[30] C.N.R. Rao, B. Raveau, Colossal Magnetoresistance, Charge Ordering, and Related Properties of Manganese Oxides, World Scientific, Singapore, 1998.
[31] C.N.R. Rao, J. Phys. Chem. B 104 (2000) 5877.
[32] J. Laugier, B. Bochu, Celref v3, Laboratoire des Materiaux et du Génie Physique de l'Ecole Supérieure de Physique de Grenoble (2003) http://www.inpg.fr/LMGP.
[33] J. Rodriguez-Carvajal, in: Collected Abstracts of Powder Diffraction Meeting, Toulouse, 1990. p. 127.
[34] K. Knížek, J. Hejtmánek, Z. Jirak, C. Martin, M. Hervieu, B. Raveau, G. André, F. Bourée, Chem. Mater. 16 (2004) 1104.
[35] F. Damay, C. Martin, M. Hervieu, A. Maignan, B. Raveau, G. André, F. Bourée, J. Magn. Magn. Mater. 184 (1998) 71.

[36] P.M. Woodward, T. Vogt, D.E. Cox, A. Arulraj, C.N.R. Rao, P. Karen, A.K. Cheetam, Chem. Mater. 10 (1998) 3652.
[37] S. Soltanian, X.L. Wangm, H.K. Liu, J. Horvat, T. Silver, S.X. Dou, Physica C 364–365 (2001) 343.
[38] V. Caignaert, F. Millange, M. Hervieu, E. Suard, B. Raveau, Solid State Comm 99 (1996) 173.
[39] E.J. Cussen, P.D. Battle, Chem. Mater. 12 (2000) 831.
[40] P.D. Battle, T.C. Gibb, C.W. Jones, J. Solid State Chem. 74 (1988) 60.
[41] S. Zouari, L. Ranno, A. Cheikh-Rouhou, O. Isnard, M. Pernet, P. Wolfers, P. Strobel, J. Alloys Compd. 353 (2003) 5.
[42] V.M. Goldschmidt, Skrifter Norske Videnskaps-Akad. Oslo, I. Mat.-Naturv. K1 (1926) 8.
[43] J.P. Attfield, Chem. Mater. 10 (1998) 3239.
[44] C. Laberty, A. Navrotsky, C.N.R. Rao, P. Alphonse, J. Solid State Chem. 145 (1999) 77.
[45] E. Takayama-Muroachi, A. Navrotsky, J. Solid State Chem. 72 (1988) 244.
[46] L. Rørmark, S. Stølen, K. Wiik, T. Grande, J. Solid State Chem. 163 (2002) 186.
[47] I.I. Daikonov, K.V. Ragnarsdottir, B.R. Tagirov, Chem. Geol. 151 (1998) 327.
[48] K.R. Poeppelmeier, M.E. Leonowicz, J.C. Scanlon, J.M. Longo, W.B. Yelon, J. Solid State Chem. 45 (1982) 71.
[49] H.G. Giesbe, W.T. Pennington, J.W. Kolis, Acta Cryst. C 57 (2001) 329.
[50] R.D. Shannon, Acta Cryst. A 32 (1976) 751.